Lawrence Berkeley National Laboratory

LBL Publications

Title
Development of a nanoindenter for in-situ transmission electron microscopy

Permalink
https://escholarship.org/uc/item/9bt8b7sr

Journal
Microscopy and Microanalysis, 7(06)

Author
Dahmen, Ulrich

Publication Date
2001-01-30

eScholarship.org Powered by the California Digital Library
University of California

Development on a nanoindenter for *in-situ* transmission electron microscopy

Eric A. Stach,[1] Tony Freeman,[2] Andrew M. Minor,[3,4] Doug K. Owen,[1] John Cumings,[4,5] Mark A. Wall,[6] Tomas Chraska,[7] Robert Hull,[7] J. W. Morris Jr.,[3,4] A. Zettl,[4,5] and Ulrich Dahmen[1]

1 National Center for Electron Microscopy, Materials Sciences Division, Lawrence Berkeley National Laboratory, Berkeley, CA 94720

2 Engineering Department, Lawrence Berkeley National Laboratory, Berkeley, CA 94720

3 Department of Materials Science and Engineering, University of California at Berkeley, Berkeley, California 94720

4 Materials Sciences Division, Lawrence Berkeley National Laboratory, Berkeley, California 94720

5 Department of Physics, University of California at Berkeley, Berkeley, California 94720

6 Chemical and Materials Sciences Directorate, Lawrence Livermore National Laboratory, Livermore, CA 94550

7 Department of Materials Science and Engineering, University of Virginia, Charlottesville, VA 22903

Corresponding author:
Eric A. Stach
National Center for Electron Microscopy
Mail Stop 72-150
1 Cyclotron Rd
Lawrence Berkeley National Laboratory
Berkeley, CA 94720
email: EAStach@LBL.gov
phone: 510.486.4634
fax: 510.486.5888

Abstract

In-situ transmission electron microscopy is an established experimental technique that permits direct observation of the dynamics and mechanisms of dislocation motion and deformation behavior. In this paper, we detail the development of a novel specimen goniometer that allows real time observations of the mechanical response of materials to indentation loads. The technology of the scanning tunneling microscope is adopted to allow nanometer scale positioning of a sharp, conductive diamond tip onto the edge of an electron transparent sample. This allows application of loads to nanometer-scale material volumes coupled with simultaneous imaging of the material's response. The emphasis in this paper is qualitative and technique-oriented, with particular attention given to sample geometry and other technical requirements. Examples of the deformation of aluminum and titanium carbide as well as the fracture of silicon will be presented.

Introduction

In-situ transmission electron microscopy (TEM) has a long history of elucidating the mechanisms of deformation in materials. The utility of electron microscopy in understanding the dynamics of dislocation behavior and material deformation stems from its ability to image in real time and at high resolution changes in dislocation structure, deformation twinning, and grain boundary motion. In the particular case of dislocations one can determine the evolution of dislocation configurations, as well as the mechanisms of nucleation, propagation, multiplication and interaction. The first real time TEM experiments studying dislocation behavior date to the late 1950's and early 1960's, when a number of *in-situ* straining stages were constructed for the intermediate and high voltage machines of that era (see Hale and Butler, 1981 for a review). These efforts continue today, and many laboratories have either home-built or commercially purchased straining stages.

Over the past five years, Wall and Dahmen have spearheaded efforts toward the development of a new methodology for observing the deformation response of materials in real time, that of *in-situ* nanoindentation (Wall and Dahmen, 1995, 1997, 1998a, 1998b). Their work to date has focused on the development of a stage for the Kratos 1.5 MeV high voltage electron microscope (HVEM) at the National Center for Electron Microscopy in Berkeley. The Kratos HVEM is well suited for studies of this type due to its high specimen penetration and large pole gap. In this original holder design, a sharp diamond tip was mounted onto a long, stiff metal rod that ran through the shaft of the goniometer (See Figure 1). This shaft pivoted about a four-point bearing surface located near the front end of the rod, with a lever arm reduction of approximately 10 to 1. Tip motion along the x and y axes was accomplished by screw piezo drives which

pushed upon bellows, while the in-and-out (or *z*-axis) control utilized an ultra-low reduction gear motor drive for tip positioning, in series with a piezoceramic stack for indentation. Wall and Dahmen presented preliminary results of *in-situ* nanoindentation of silicon using this holder (Wall and Dahmen, 1998a). Chen et al. (1997) demonstrated the applicability of this technique toward understanding the mechanical behavior of carbon nanotubes.

Recently, a number of investigators have constructed *in-situ* transmission electron microscopy stages which adapt the technology of scanning tunneling microscopes to allow nanoscale positioning and probing of materials (Kizuka et al., 1997; Ohnishi et al., 1998; Wang et al., 1999; Cumings and Zettl, 2000; Lin and Dravid, 2000). In the cases of Kizuka et al. and Ohnishi, et al. these stages have been utilized to investigate atomic scale contacts and quantum effects in the conductivity of angstrom-scale gold wires. The experimental work of Wang, Cumings and Zettl, and Lin and Dravid has focused on fundamental properties of carbon nanotubes. Generally, all of these stages utilize a piezoceramic tube for 3-axis positioning of a sample against a static contact point. Each of these experiments requires high image resolution and the precise sample control that a piezoceramic manipulator permits.

In this paper, we describe our continuing development of the *in-situ* nanoindentation technique. Building upon the aforementioned developments, we have constructed a new nanoindenter for a 200 keV JEOL 200CX transmission electron microscope which combines accurate positioning control using the piezoceramic method with dedicated indentation capabilities. This stage allows room temperature deformation of both focused ion beam (FIB) prepared and microfabricated silicon samples using a permanently mounted Berkovich diamond indenter. We will first describe in detail the construction of the nanoindenter. A description of

the sample requirements and geometries will follow. Thereafter, we will present some of our observations of the room temperature indentation of several different materials.

Experimental

Holder construction

Figure 2 presents a schematic of the new room temperature *in-situ* nanoindenter, which was designed for use in a JEOL 200 CX TEM. Figure 3 presents a photograph of the device. This holder has several significant differences from the model of Wall and Dahmen, which was designed for the Kratos HVEM. Firstly, the coarse positioning of the indenter tip in all three axes is accomplished with manual screw drives that push against the bellows assembly. This is in contrast to the prior design, which used screw drives for coarse x and y motion and a fine gear motor for coarse z motion. In the current version, it is possible to position the tip mechanically to within about one micron of the electron transparent edge using the coarse z controls. Positioning of the tip along x and y has a similar degree of mechanical control, but the fact that the image is a transmission image makes it difficult to locate the tip at the right "height" (y) in the microscope for indentation using only the mechanical controls.

Fine motion of the tip is controlled in all three axes with the piezoceramic tube. This allows increased ease and precision of tip positioning, which is a critical experimental parameter. In order to accomplish this three-axis positioning, electrical contacts are made to four mutually orthogonal sides of the piezo (See Figure 4). The x and y axes are controlled independently by varying the voltage across the coupled pairs indicated, while the z motion is controlled by varying the voltage across all four wires simultaneously. With this method it is possible to position the tip with $\approx$ 1 nm precision.

Sample geometry

Sample preparation is a critical component of these *in-situ* nanoindentation experiments. We have prepared successful samples in two ways: by focused ion beam etching (FIB) and by thin film deposition on microfabricated silicon templates. These two sample geometries are significantly different; we have, therefore, modified the sample holder to accept removable front pieces that accommodate the different sample types.

(i) Focused ion beam samples

In situ nanoindentation in a TEM requires a sample geometry such that the electron-transparent section can be approached by the diamond indenter in a direction normal to the electron beam. In the FIB sample, this is accomplished by cutting trenches into the sample that define an electron-transparent window. Figure 5(a) shows a schematic of the geometry of the FIB sample with respect to the electron beam and indenter, while 5(b) is a very low magnification TEM image of the indenter and a typical FIB specimen. The focused ion beam method is ideally suited for the preparation of bulk materials for *in-situ* nanoindentation. This is because nearly all materials can be made electron transparent in a suitable geometry using this technique.

Figure 6 is an optical micrograph of the tip piece used to hold the FIB samples during indentation. The FIB "half grids" are attached to the semicircular shelf with conductive carbon paint. It is possible to manually tilt this shelf *ex-situ* ± 15° in order to ensure that the electron beam is nearly perpendicular to the membrane surface. This is necessary because the aspect ratio of a typical FIB trench is on the order of 10 : 1. Thus, without the *ex-situ* tilt, it is very difficult to place the sample on the shelf in such a way that the surface of the electron transparent

membrane is parallel to the shelf surface. If the membrane is not almost exactly perpendicular to the electron beam, the sample bulk overhangs the electron transparent region, obscuring the area of interest.

Although focused ion beam preparation allows the production of suitable samples from nearly any bulk material, it has three particular disadvantages. The first disadvantage is the relative lack of availability of FIB machines for sample preparation. The resulting shortage of samples substantially limits the number of indentations that can be performed on a given materials system, and thus the ability to do systematic experimentation. Secondly, only one axis of tilt is available during imaging (the second tilt requires removal of the holder from the microscope and manual manipulation with a pair of tweezers). Because of the trench geometry of FIB samples, only about ± 5° tilt is available along this axis. This greatly limits the possible diffraction conditions available for quantitative characterization of dislocations. Finally, the FIB membrane geometry is not a very rigid one. We have observed that some FIB membranes may bend during indentation, fundamentally altering the experiments (two examples will be discussed in detail below). However, we do find that FIB samples of materials with high elastic moduli are sufficiently rigid and do not bend during indentation.

(ii) Microfabricated silicon samples

In order to address the aforementioned difficulties associated with FIB samples, we have developed a second method of sample preparation following the suggestions of Wall and Dahmen (1998b). In this method we exploit traditional lithographic silicon fabrication techniques to create electron transparent wedge-shaped samples of well-defined geometry and orientation. As shown schematically in Figure 8 and explicitly in Figure 9, the new sample

design consists of small "H's", in which the crossbar of the H is a sharp silicon ridge of (111) planes. The planes meet at the top, where the small radius of curvature leads to approximately ~250-400 nm of electron transparency at 200kV.

This new sample design has at least five distinct advantages over the FIB-prepared samples for *in situ* nanoindentation:

(1) The silicon ridge sample design allows for the examination of many different materials through the use of a common silicon substrate and thin film deposition techniques. Figure 8(b) shows an example of this, in which a thin film of Al has been deposited on top of the silicon substrate.

(2) The increased rigidity due to the sloped shape of the ridges leads to little or no bending during indentation, both with and without thin films on top of the substrates.

(3) The length of the sharp silicon ridge (1.5 mm) allows for many indentations to be made on a single sample.

(4) The ridge sample design allows for a large angle of rod-axis tilt in the TEM, allowing detailed examination of dislocation structure in the indented region.

(5) The film is deposited over a large flat region as well. This allows *ex-situ* indentation experiments to be performed on the same sample using a commercial nanoindentation system, allowing direct comparison between our *in-situ* experiments and standard analyses.

Results

Bulk aluminum (FIB)

Initial experiments to test the functionality of the nanoindentation holder used pure aluminum. The sample was prepared using the focused ion beam method, with a nominal membrane thickness of approximately 500 nm. A time sequence of images taken from one indentation of this sample is shown as Figure 10. In Figure 10(a) we see the sample and tip geometry at the beginning of the indentation. In Figure 10(b) through (f) we track the microstructural evolution of the material's response to deformation. These images were taken at relatively low magnifications in order to observe the behavior of a larg area of the sample.

What is most readily apparent in these images is the motion of bend contours through the thin foil as indentation proceeds. Bend contours are a diffraction phenomenon which arises from the change in orientation of particular sets of planes within the sample relative to the electron beam. Therefore, real time observations of bend contour movement map out the bending of planes as a function of indentation displacement. Two effects may contribute to bend contour motion:

a) Bending of planes due to elastic and plastic strains induced in the material by the motion of the indenter. This is the 'real effect' of nanoindentation.

b) Slight buckling of the thin FIB membrane. This is an artifact resulting from the thinness of the foil, and obfuscates our observations of the true effects of the nanoindentation itself.

It is not possible in this case to be certain whether or not buckling is occurring in this series or if all of the observed bending of planes is due to a proper indentation response. However, it seems

quite possible that buckling does occur as a result of the relatively low elastic modulus of aluminum.

Throughout the indentation, the nucleation and propagation of dislocations underneath the indenter tip is observed, as "geometrically necessary" dislocations are introduced to accommodate the shape change imposed in the material by the indenter (Nix, 1997). Additionally, we find that following nucleation, dislocations propagate far into the film, stopping only when they interact with other dislocations. Each of these observations is unaffected by possible artifacts associated with sample bending.

Bulk titanium carbide (FIB)

Figure 11 is a video tableau from the indentation response of a 500 nm thick FIB prepared titanium carbide (TiC) sample. Unlike the case of pure aluminum, no significant motion of bend contours is visible across the main part of the sample during indentation. Instead, the deformation response is localized to a region within about 500 nm of the indenter tip. Titanium carbide is an extremely hard material, with a high elastic modulus. As a result, the sample is much less susceptible to buckling, and statements about the indentation response can be made with less concern for artifacts.

The most obvious difference between the behavior of TiC and aluminum is the extent to which dislocations, once nucleated, propagate into the sample bulk. Because of the strong bonding in TiC, the Peierls stress (which is the magnitude of stress that must be applied in order to move a dislocation through the crystal) is correspondingly large, on the order of 7.3 GPa compared with 860 MPa in aluminum (Krenn, et al. 1998). Considering the classic elasticity solution of Hertz for two bodies in contact, the maximum shear stress in the material underneath

the indenter tip falls of as $\sqrt[3]{1/r^2}$ (Timoshenko and Goodier, 1969). Thus, it is likely that the reason that dislocation motion does not extend deep into the crystal is that beyond a given distance, the applied stress in the crystal has fallen below the Peierls stress. We are presently working to calibrate the load applied by the indenter as a function of the voltage applied to the piezoceramic tube. This will allow us to quantitatively characterize the fundamental processes of dislocation nucleation and motion in the hard transition metal carbonitrides.

Bulk silicon (FIB)

In Figure 12, we present another tableau of video images taken from an indentation of a pure silicon FIB sample. In this series, the tip of the indenter did not meet the sample edge directly in the center, but rather was slightly underneath the plane of the sample (or above - it is not possible to tell which in a transmission image). So, as the indenter was driven in the indentation (z) direction, the sample was both indented and bent at the same time. Despite this, certain useful information can be obtained from this series.

Firstly, as is quite evident, sufficient force can be applied to materials by the *in-situ* nanoindenter to both nucleate and propagate cracks in strong, brittle materials. In this case, as expected, the sample cracked along a {111} type plane in the material. *Ex post facto* observations of the cracked region did not show either dislocation nucleation or a stress-induced phase transformation (Pirouz et al. 1990). Additionally, very clear motion of bend contours underneath the tip can be observed throughout the series. Because the material is single crystal silicon, the bend contour motion can be followed in a more systematic manner than in the polycrystalline aluminum shown as Figure 10. Recent work by Janssen et al. and Demarest et al. has shown that it is possible to quantitatively characterize the stresses present in a material by

correlating finite element models of stress distributions with quantitative diffraction contrast image simulations. In future work, we hope to utilize these techniques to quantify the evolution of internal stresses as a function of indentation depth.

Aluminum film on microfabricated silicon ridges

Our final tableau of video images is shown as Figure 13. The sample here is a 200 nm thick aluminum film which has been evaporated onto one of the microfabricated ridge samples described above. In this case, the substrate was held at a temperature of 300 °C during deposition to promote a large grain size in the film. In this experiment, we have chosen to image only one grain in a strong two-beam dark field condition. Therefore, the indenter itself is not well illuminated, but its position is represented by an arrow in Figure 13(a). In Figure 13(b) we see the presence of a distinct set of geometrically necessary dislocations which has nucleated beneath the indenter tip. Once nucleated, these dislocations glide to the interface between the aluminum film and the silicon substrate. In Figure 13(c) through (f), we monitor the dislocation array with increasing penetration depth, noting in particular the pile-up of dislocations at the interface.

It has been observed that the hardness of metal films on rigid substrates can greatly exceed the hardness of the same materials in bulk form, and that the hardness increases as the film thickness decreases (Doerner et al. 1986). It has been proposed that the large gradients in strain that develop underneath the indenter tip result in significant densities of geometrically necessary dislocations being introduced into the film. The increased numbers of dislocations harden the material, both through dislocation – dislocation interactions, as well as dislocation – substrate interactions (Fleck and Hutchinson, 1993; Nix and Gao, 1998). We are presently doing

systematic measurements of the density of dislocations introduced into the material as a function of indentation depth in films of varying thickness. This will allow experimental determination of the role of the various interaction processes in increasing the hardness of thin films.

Conclusions and future developments

We have detailed the development of a novel specimen goniometer for *in-situ* transmission electron microscopy observations of the nanoindentation of materials. Emphasis has been placed on the operation of the holder and sample requirements. Initial experiments focusing on the deformation behavior of aluminum, titanium carbide, silicon and aluminum films on silicon have been presented. These have demonstrated the applicability of the technique for observing the nucleation, propagation and interaction of dislocations in these materials, as well brittle fracture.

This technique is still in the early stages of development. Ongoing technical improvements include quantification of the load applied as a function of the voltage to the piezoceramic tube. This will permit direct correlation of our *in-situ* observations with standard load - displacement curves typical of conventional nanoindentation experiments. Additionally, we have nearly completed a second goniometer that permits heating of both the sample and the tip. At present, sample temperatures in excess of 550 °C have been obtained, and tip temperatures up to 300 °C. We are actively modifying the design of this holder to permit sample and tip temperatures on the order 1000 °C. This will allow us to observe the deformation-induced motion of dislocations in materials with high Peierls barriers, such as semiconductor materials and the hard transition metal carbonitrides.

Acknowledgements:

This work was supported by the Director, Office of Energy Research, Office of Basic Energy Sciences, Materials Science Division of the U.S. Department of Energy under Contract No. DE-AC03-76SF000098. The authors would like to thank K. McIlwrath of Nissei Sangyo America for assistance with the TiC FIB sample preparation and D.C. Chrzan for many suggestions and insights.

References

Binning G, Rohrer H, Gerber C, Weibel W (1982) Surface studies by scanning tunneling microscopy. Phys Rev Lett 49:57-61.

Chen S-J, Ritchie R, Zettl A, Dahmen U (1998) *In-situ* bending deformation of carbon nanotubes in a HVEM. Proc. ICEM 14:75-76.

Cumings J, Zettl A (2000) Low-friction nanoscale linear bearing realized from multiwall carbon nanotubes. Science, 289:602-4.

Demarest J, Hull R, Schonenberg KT, Janssens, KGF (2000) Nanoscale characterization of stresses in semiconductor devices by quantitative electron diffraction. Appl. Phys. Lett. 77:412-14.

Doerner MF, Gardener DS, Nix WD (1986) Plastic properties of thin films on substrates as measured by submicron indentation hardness and substrate curvature techniques. J. Mater. Res. 1:845-51.

Fleck NA and Hutchinson JW (1993) A phenomenological theory for strain gradient effects in plasticity. J. Mech. Phys. Solids 41:1825-57.

Hale KF, Butler EP (1981) Dynamic experiments in the electron microscope In: *Practical Methods in Electron Microscopy*, vol 9. Glauert, AM (ed). Amsterdam: North-Holland Publishing Company.

Janssens KGF, Van Der Biest O, Vanhellemont J, Maes HE (1997) Assessment of the quantitative characterization of localized strain using electron diffraction contrast imaging. Ultramicroscopy 69:151-67

Kizuka T, Yamada K, Deguchi S, Naruse M, Tanaka N (1997) Cross-sectional time-resolved high-resolution transmission electron microscopy of atomic-scale contact and noncontact-type scannings on gold surfaces. Phys Rev B 55:R7398-401.

Krenn, CR, Morris JW Jr., Jhi, S-H, Ihm, J (1998) Relationship between atomistic bonding and intrinsic macroscopic hardness. In: *Hard coatings based on borides, carbides and nitrides: synthesis, characterization and applications*, Kumar A, Chung Y.-W, Chia RWJ (eds). Warrendale, PA, USA: TMS pp. 379-88.

Lin X and Dravid VP, submitted work.

Pirouz P, Chaim R, Dahmen U, Westmacott KH (1990) The martensitic transformation in silicon. I. Experimental observations. Acta Metall. Mat.38:313-22.

Nix WD (1997) Elastic and plastic properties of thin films on substrates: nanoindentation techniques. Mat. Sci. Eng. A 234-236:37-44

Nix WD and Gao H (1998) Indentation size effects in crystalline materials: A law for strain gradient plasticity. J. Mech. Phys. Solids 46:411-425.

Ohnishi H, Kondo Y, Takayanagi K (1998) UHV electron microscope and simultaneous STM observation of gold stepped surfaces. Surface Science 415:L1061-4.

Timoshenko, SP, Goodier, JN (1969) *Theory of Elasticity*, 2nd ed. New York: McGraw Hill.

Wall MA, Barber TW Jr, Dahmen U (1995) Techniques for *in-situ* HVEM mechanical deformation of nanostructured materials. Proc. MSA 53:240-1.

Wall MA, Dahmen, U (1997) Development of an *in-situ* nanoindentation specimen holder for the high voltage electron microscope. Microscopy & Microanalysis, 3:593-4.

Wall MA, Dahmen U (1998a) *In-situ* nanoindentation of Si in the high voltage electron microscope. Proc. ICEM 14:493.

Wall MA, Dahmen U (1998b) An *In-situ* nanoindentation specimen holder for a high voltage transmission electron microscope. J. Micr. Res. Techn. 42:248.

Wang ZL, Poncharal P, De Heer, WA (199) Measuring physical and mechanical properties of individual carbon nanotubes by *in-situ* TEM. J Phys Chem Solids, 61:1025-30.

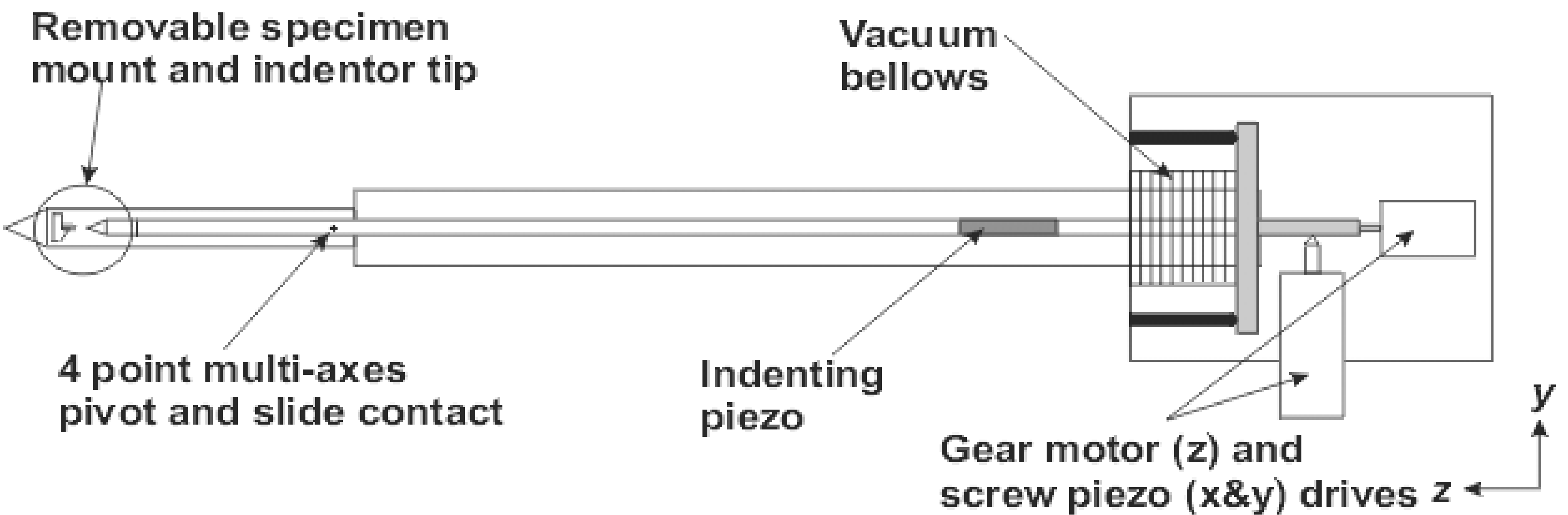

Figure 1 Schematic of original *in-situ* nanoindentation holder for the Kratos HVEM (adapted from Wall and Dahmen, 1998b).

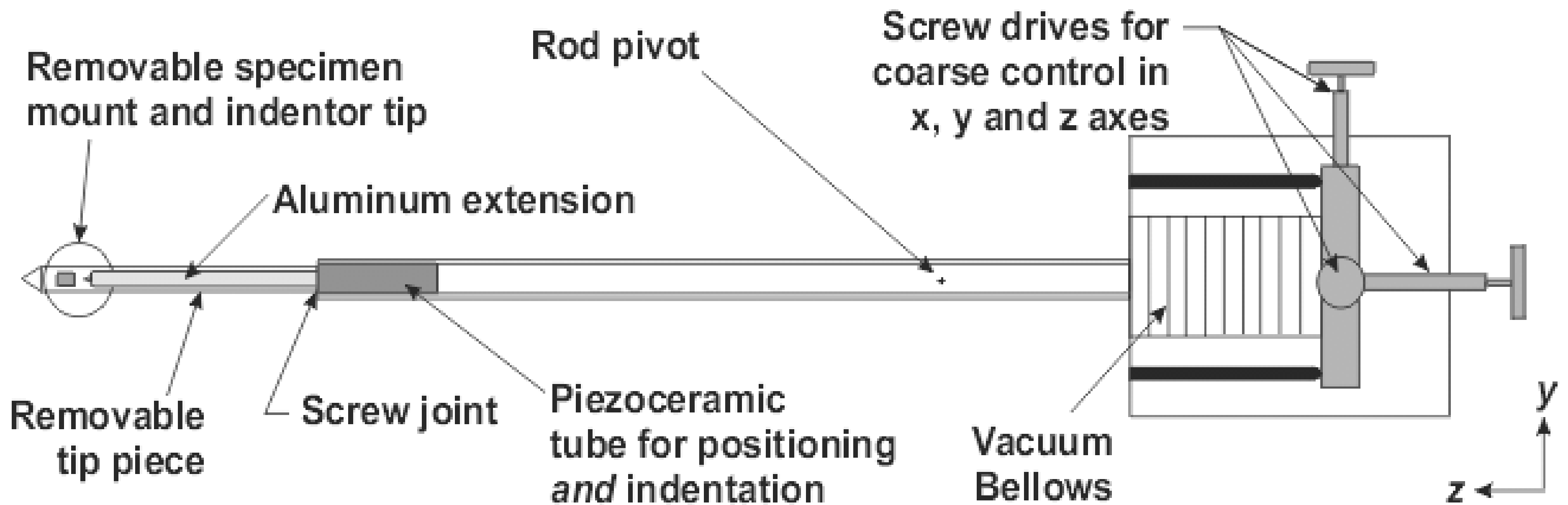

Figure 2 Schematic of *in-situ* nanoindentation holder for JEOL 200CX "*In-situ* microscope"). Electron beam travels in the *y* direction.

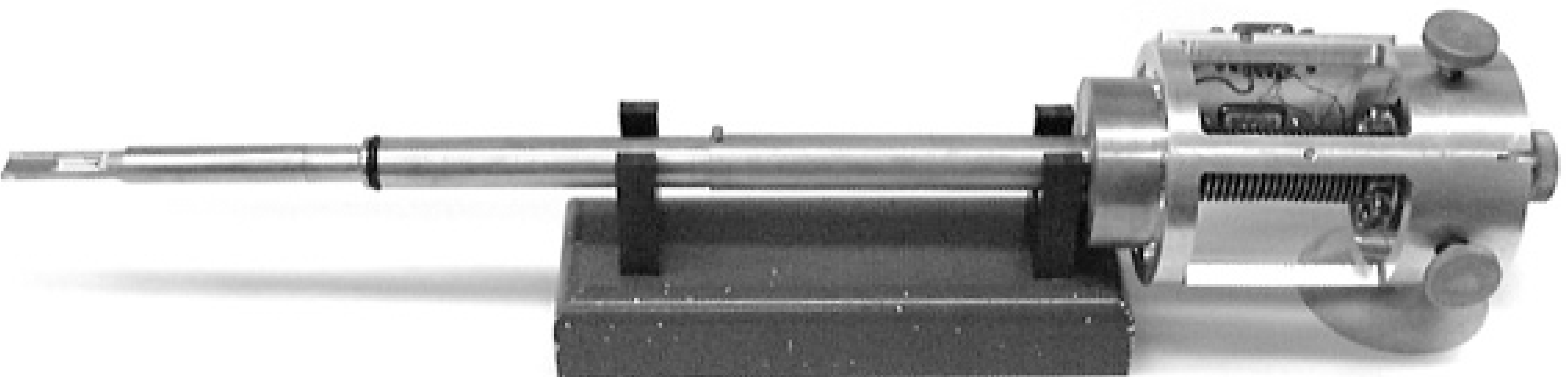

Figure 3 *In-situ* nanoindentation holder for JEOL 200CX "*In-situ* microscope"

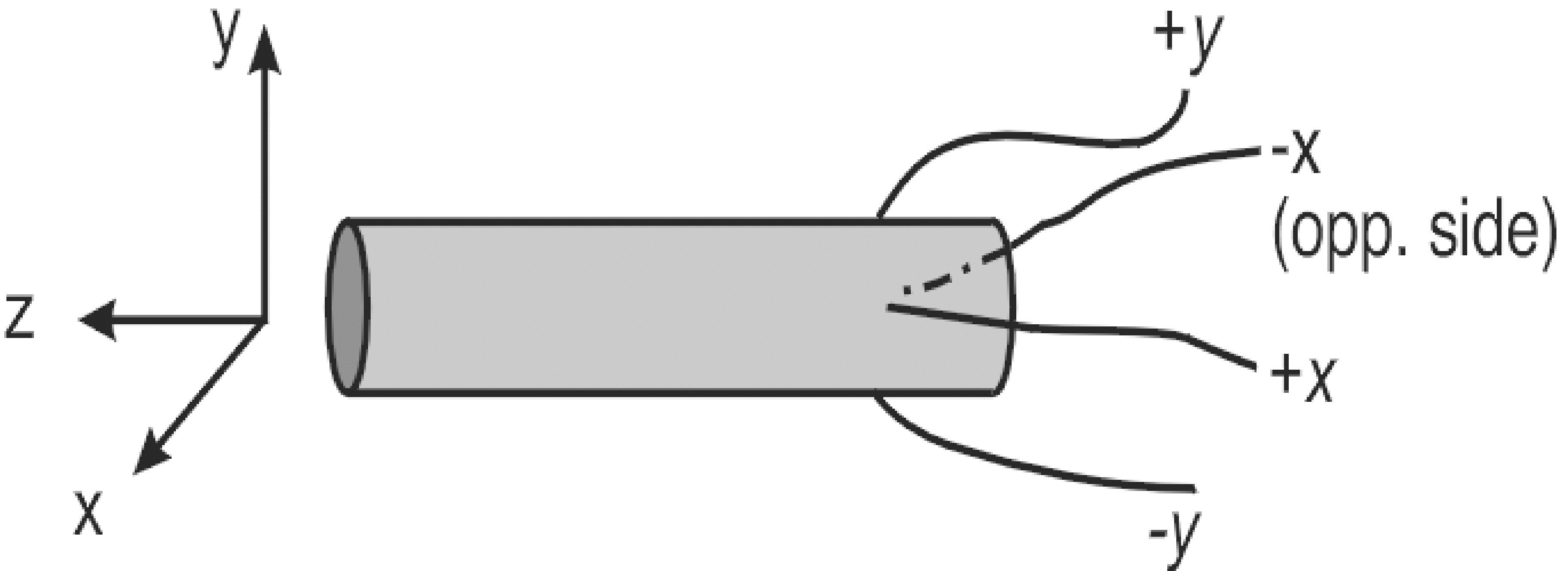

Figure 4 Schematic wiring diagram for piezoceramic tube.

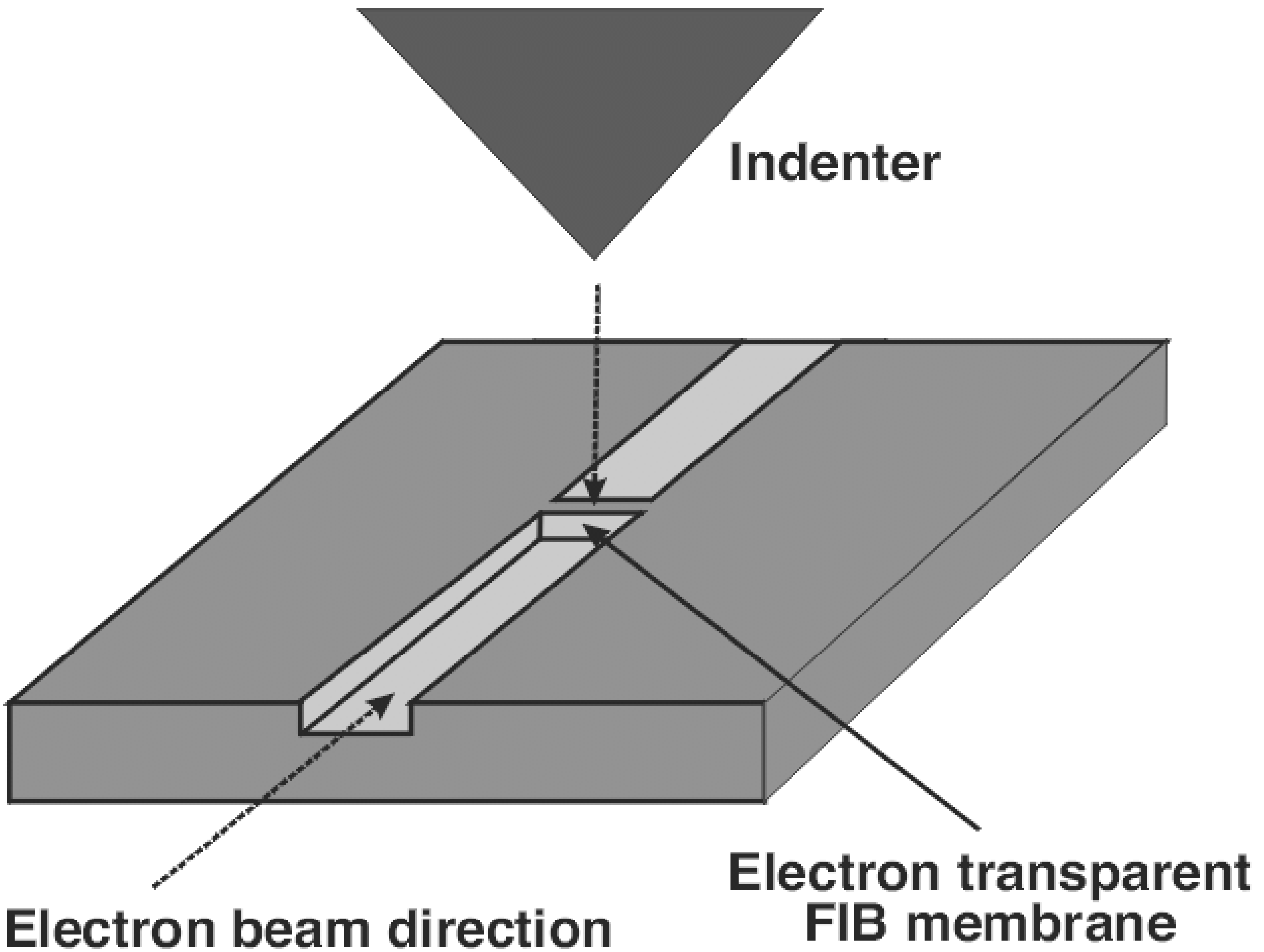

Figure 5 (a) Schematic of the FIB-TEM experimental geometry.

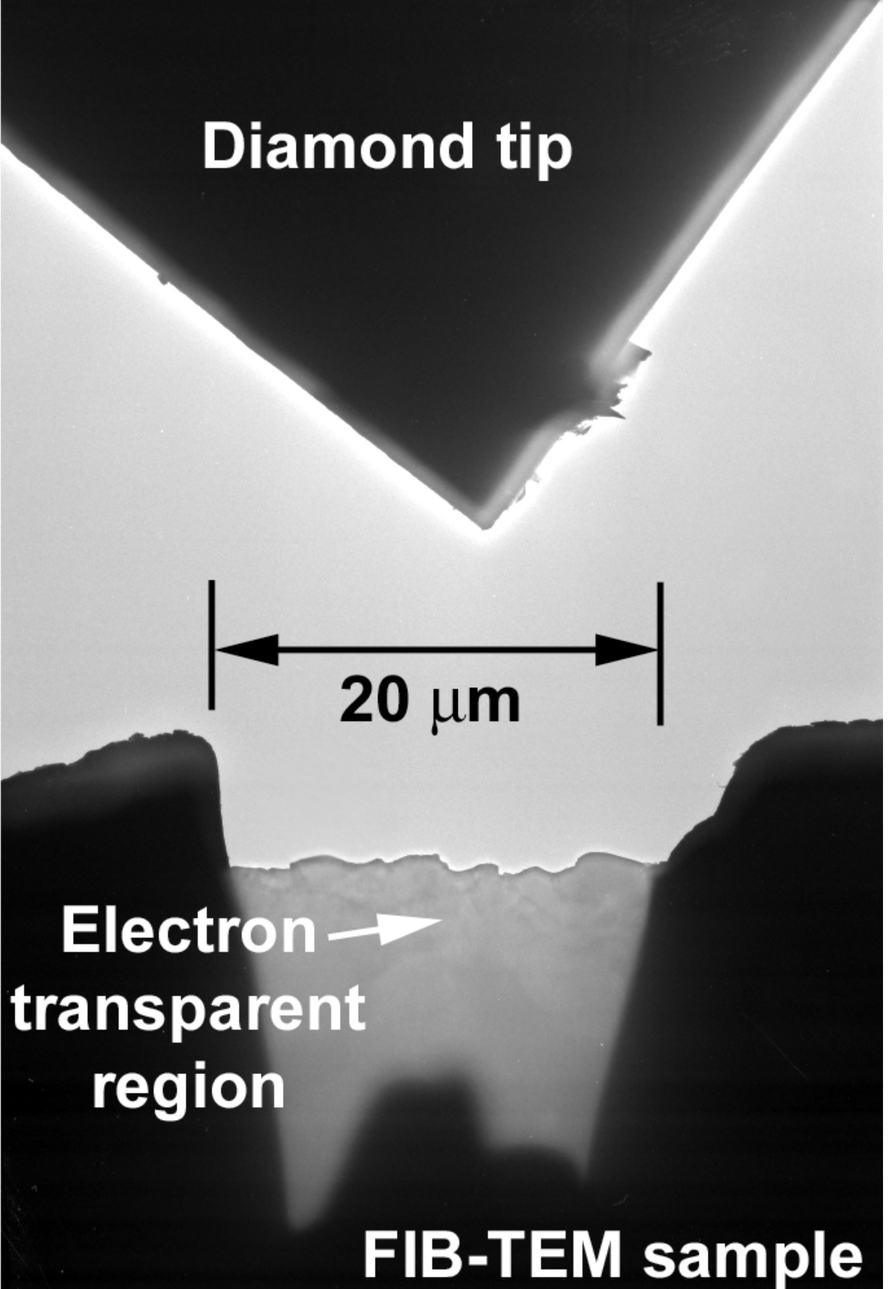

Figure 5 (b) A typical low magnification image showing the indenter tip and electron transparent region of a FIB prepared sample.

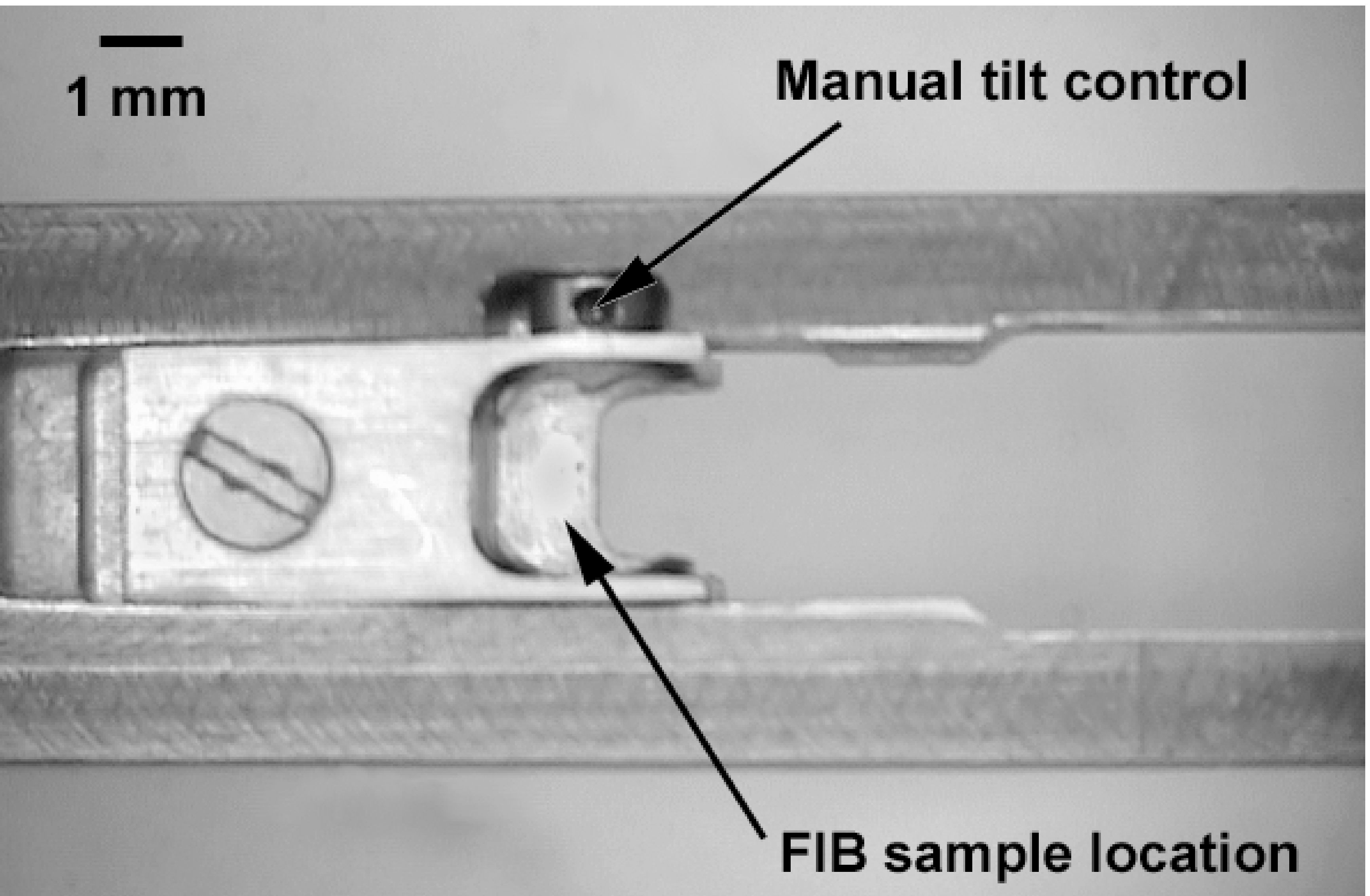

Figure 6 Sample mount geometry for FIB prepared samples.

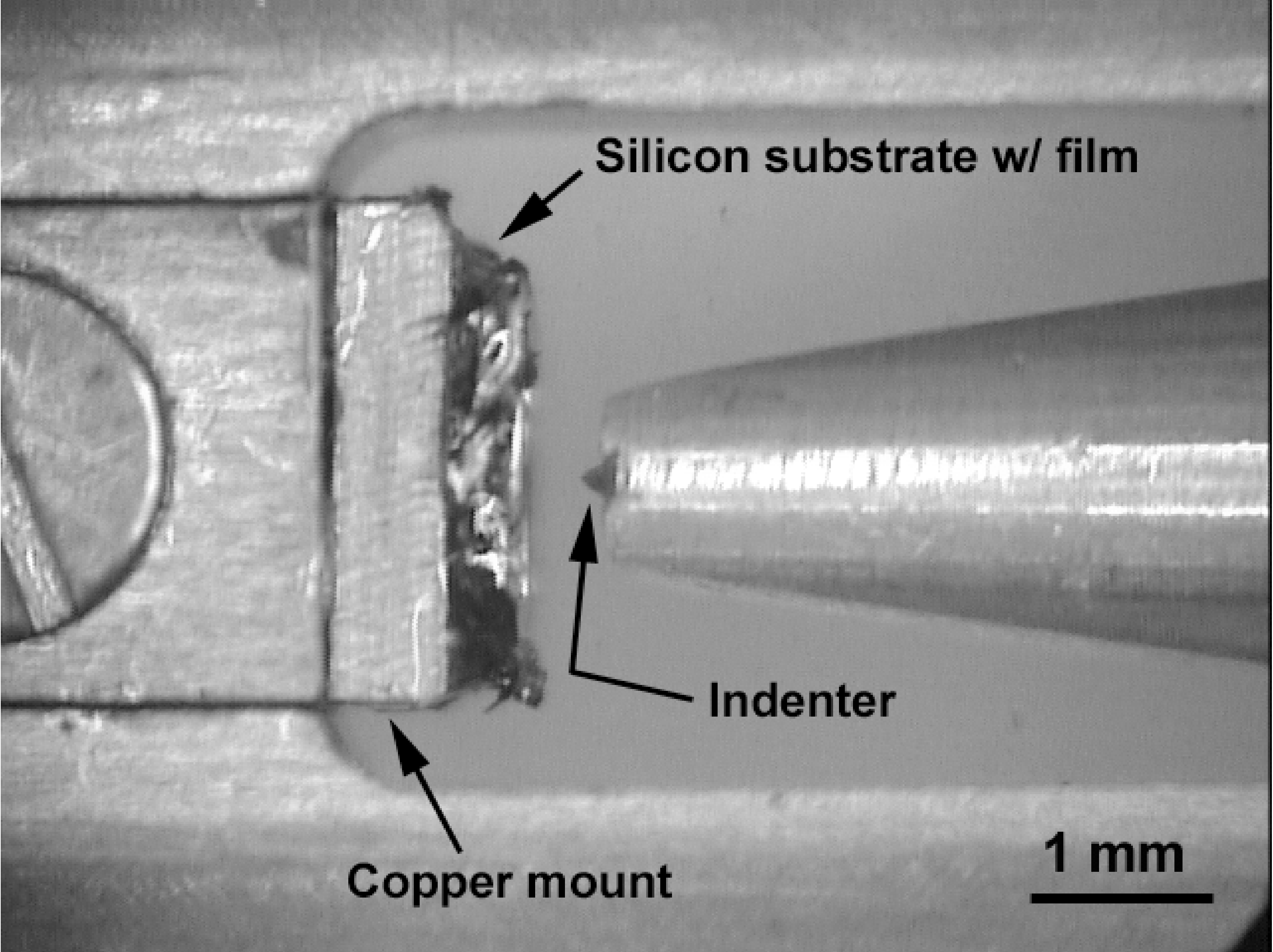

Figure 7 Sample mount geometry for lithographically prepared silicon samples.

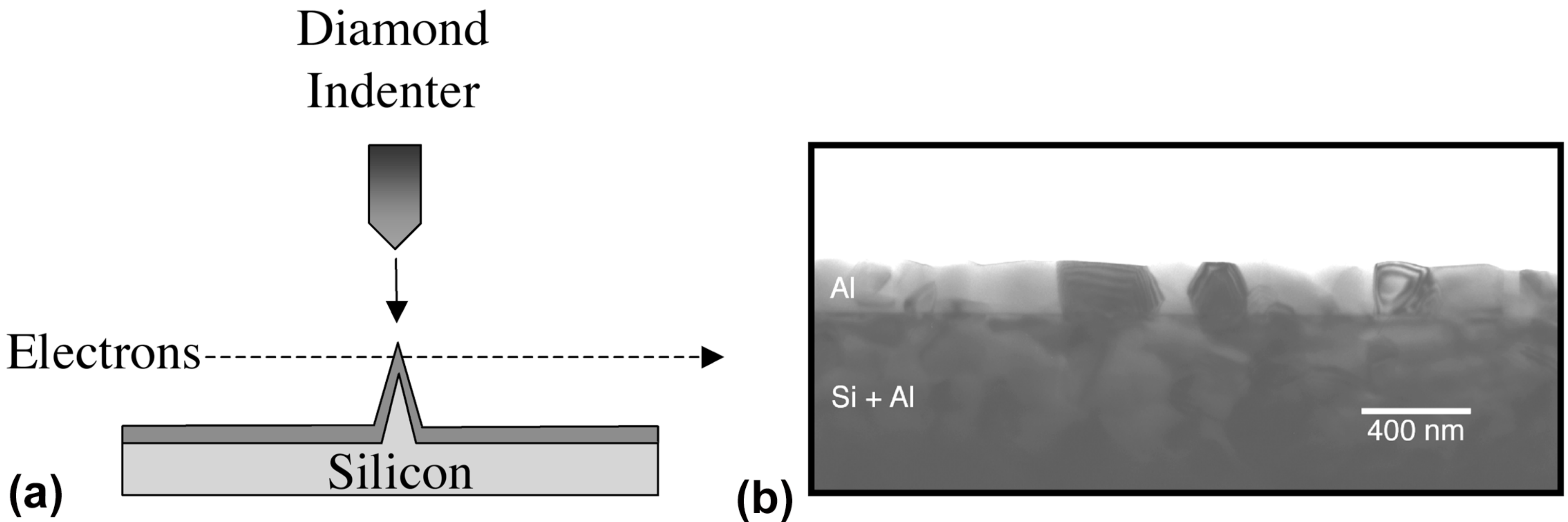

Figure 8 (a) Schematic of microfabricated sample and viewing geometry. (b) Example image from a sample of aluminum deposited onto a microfabricated Si ledge.

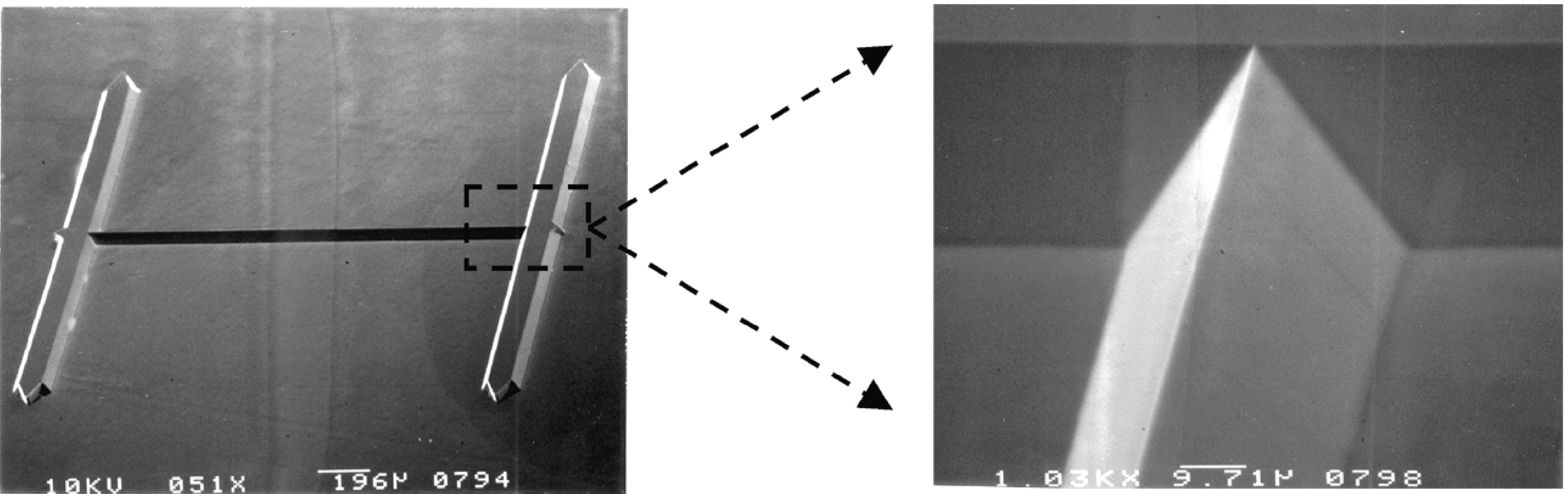

Figure 9 (a) Low magnification SEM micrograph of a microfabricated ridge sample. (b) Higher magnification of ridge region. Image (b) rotated 90º from image (a).

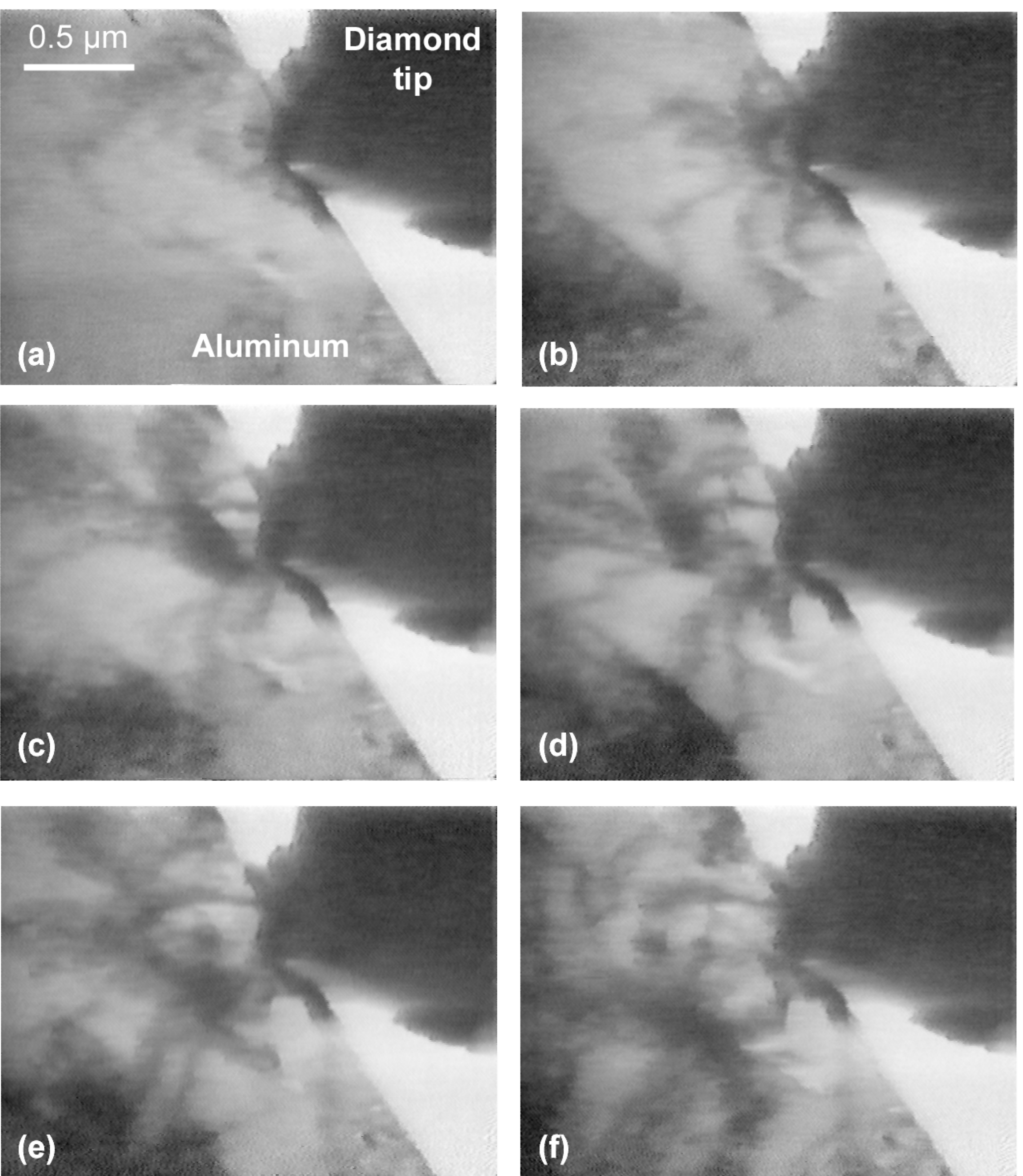

Figure 10 Series of video frames from an *in-situ* indentation of an aluminum FIB sample.

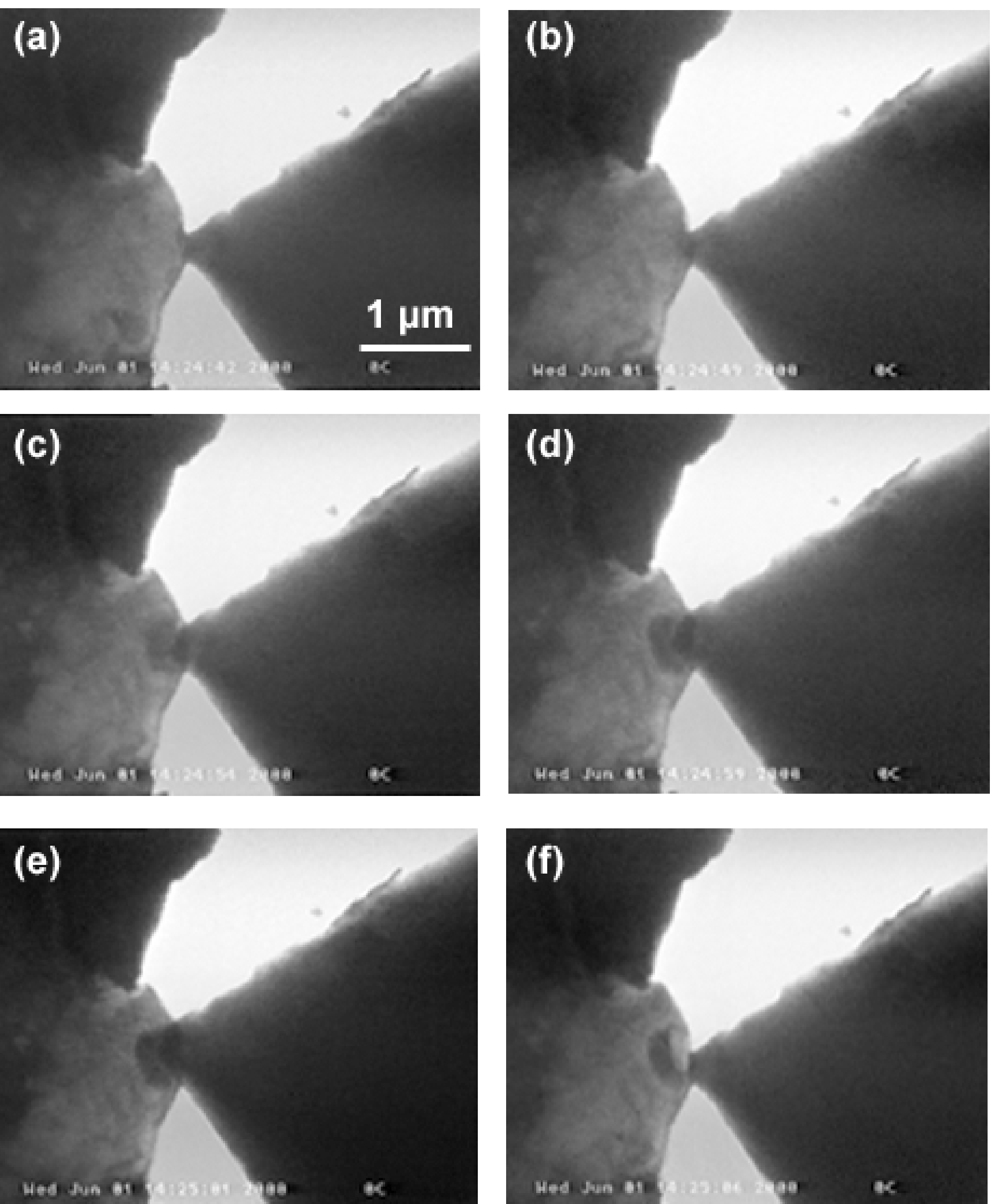

Figure 11 Series of video frames from an *in-situ* indentation of a Ti C FIB sample.

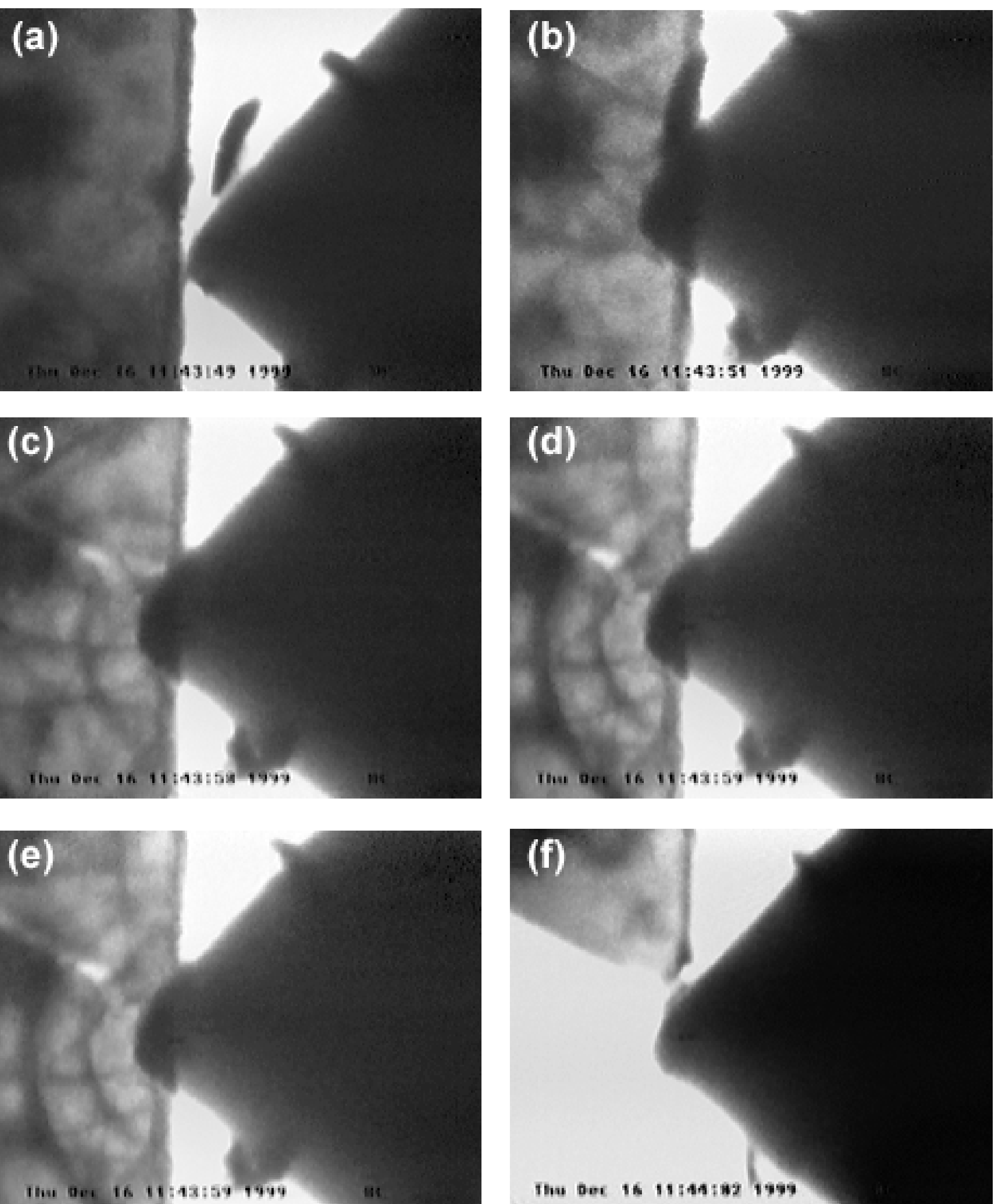

Figure 12 Series of video frames from an *in-situ* indentation of a silicon FIB sample.

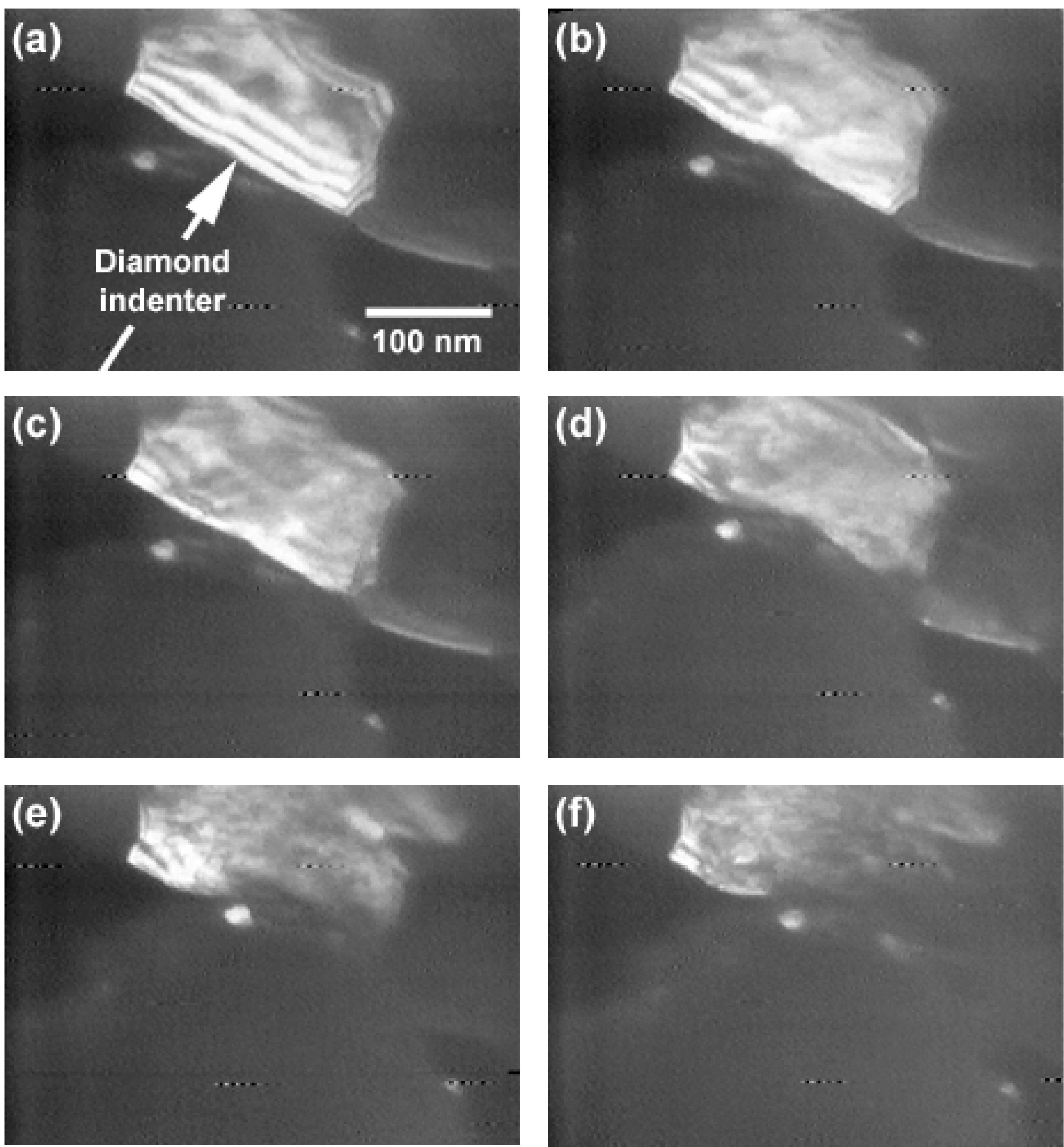

Figure 13 Series of video frames from an *in-situ* indentation of an aluminum film on a microfabricated silicon sample.